AIAA JOURNAL
Vol. 42, No. 9, September 2004

Crossflow-Induced Transition Prediction Using Coupled Navier–Stokes and e^N Method Computations

Hans W. Stock* and Arne Seitz†
DLR, German Aerospace Research Center, 38108 Braunschweig, Germany

The flow around two infinite swept wings and an infinite swept cylinder model is computed using a Reynolds averaged Navier–Stokes method coupled to a boundary-layer and transition prediction method based on the e^N approach. The configurations were wind-tunnel tested, including transition location measurements. In all test cases, transition is provoked purely by crossflow instabilities. The inifinite swept wing experiments represent critical test cases because they contradict two assumptions made in the conventional e^N approach, where the limiting crossflow N factor is supposed to be independent of the surface curvature and the quality of the wing surface finish. It will be shown that the extended version of the e^N method can resolve this problem and produce acceptable results. The infinite swept cylinder model tested at high sweep angles between 53 and 71 deg is excellently suited to demonstrate that the e^N method is capable of describing the leading-edge contamination problem. For sweep angles between 53 and 58 deg, a relative constant limiting crossflow N factor exists, whereas for higher sweep angles the crossflow N factors at the measured transition location deacrease gradually. Applying the leading-edge contamination criterion of Pfenninger, the e^N method predicts the sweep angle, where leading-edge contamination starts to influence the laminar boundary-layer flow. Furthermore, the sweep angle, which produces, according to an empirical correlation, fully turbulent leading-edge flows, is well predicted by the e^N method.

Nomenclature

C = chord length
C_{Df} = friction drag coefficient of the wing section
C_{Dp} = pressure drag coefficient of the wing section
$C_{D\text{tot}}$ = total drag coefficient of the wing section
C_L = lift coefficient of the wing section
C_p = pressure coefficient
N_{CF} = N factor of unstable stationary crossflow waves at the measured transition location
N^*_{CF} = envelope N factor of unstable stationary crossflow waves
N_{limit} = limiting N factor for unstable stationary crossflow waves
Re = Reynolds number based on chord and freestream conditions
Re_θ = Reynolds number based on the momentum loss thickness of the attachment line flow, $W_\infty \theta \rho / \mu$
U = velocity component in direction of the resultant velocity at the outer edge of the boundary layer
u = velocity component in chordwise direction
V = crossflow velocity component
W_∞ = velocity component of the freestream in spanwise direction, $U_{\text{al},e} = \text{const}$
X = coordinate in chordwise direction
Z = coordinate normal to the surface
Z_p = coordinate normal to the planform of the wing
α_n = angle of attack in a direction normal to the leading edge
α_s = angle of attack measured in the direction of the freestream, $\tan\alpha_s = \tan\alpha_n \cos\lambda$
δ^*_{ic} = incompressible value of the displacement thickness of the crossflow velocity profile, $-\int_0^\infty \frac{V}{U_e} \mathrm{d}Z$
δ^*_{is} = incompressible value of the displacement thickness of the streamwise velocity profile, $\int_0^\infty \left[1 - \frac{U}{U_e}\right] \mathrm{d}Z$
θ = momentum loss thickness of the attachment line flow, $\int_0^\infty \frac{U_{\text{al}}}{U_{\text{al},e}} \left[1 - \frac{(U_{\text{al}})}{U_{\text{al,e}}}\right] \mathrm{d}Z$
λ = sweep angle
μ = kinematic viscosity
ρ = density
$1/R$ = surface curvature, with R equal to radius of curvature

Subscripts

al = attachment line
e = outer edge of the boundary layer
Tr = transition
∞ = upstream infinity

I. Introduction

IT is well known that operational costs for transport aircraft are strongly related to the aerodynamic drag. Large surface areas on wings, tails, and nacelles covered with laminar flow will reduce the drag considerably, save fuel costs, and protect the environment. To evaluate potential savings in fuel costs or improvements in aerodynamic efficiency as a function of laminar surface area, one must be able to predict accurately the location of boundary-layer transition. The range of existing transition prediction methods extends from simple empirical relationships through different levels of stability theories [linear and local parallel flow, and nonlocal, linear or nonlinear parabolized stability equation (PSE) methods] to direct numerical simulations. The e^N method based on local, linear stability theory and the parallel flow assumption[1,2] still represents the current state of the art for transition onset prediction in the aircraft industry. The value of e^N stands for the ratio of the disturbance amplitude at transition related to the disturbance amplitude at the

Received 17 October 2003; revision received 7 April 2004; accepted for publication 12 April 2004.

*Senior Research Scientist, Institute of Aerodynamics and Flow Technology, Lilienthalplatz 7.
†Research Scientist, Institute of Aerodynamics and Flow Technology, Lilienthalplatz 7.

neutral point. The quantity N, representing the limiting N factor, is not known a priori and has to be determined by calibration of wind-tunnel or free-flight tests; hence, in this aspect the e^N approach is a semi-empirical method. On one hand, this approach is often criticized because it does not account for all fundamental aspects in the transition process, but on the other hand, there is no other practical method presently available for industrial applications.[3]

Only recently, it has been shown that Navier–Stokes methods coupled to the e^N method produce excellent results for laminar airfoils when compared to wind-tunnel measurements.[4–6] The work documented in Refs. 4–6 comprises a feasibility study,[4] the transitional flow modeling,[5] and the validation[6] for airfoil flows. The approach was applied for design studies of a laminar wing with low-leading-edge sweep in normal conditions and in situations where the wing is heated by intensive sunshine on the airfield before takeoff.[7] Finally, the approach using the Navier–Stokes code coupled to the two N factor e^N transition prediction was successfully extended to three-dimensional flows on infinite, swept wings. The feasibility study is described in Ref. 8, and the validation with experiments is given in Ref. 9. The comparison between computations and experiments on four configurations, where one configuration was tested in two different wind tunnels, was shown to be excellent.[9]

Presently, three test cases are investigated, where transition is solely provoked by unstable crossflow waves. The work is concentrated on three different aspects, first, on the influence of wing surface curvature, second, on the influence of wing surface finish, and, third, on the leading-edge contamination problem. The main emphasis is to demonstrate that the e^N method is able to cope all of these aspects.

II. Applied Computational Methods

The coupling of the Navier–Stokes method for infinite swept wing configurations with the e^N method applies four different codes for the iterative computation cycle:

1) The Reynolds averaged Navier–Stokes (RANS) equations, describing two-dimensional, unsteady, compressible flows in conservation form, are solved by means of a finite volume approach using a Runge–Kutta time-stepping method with multigrid acceleration (see Ref. 10). Leicher et al.[11] extended the code to infinite swept wing capabilities using the Baldwin–Lomax turbulence model.[12]

2) The boundary-layer method for laminar, compressible flows on swept, tapered wings[13] is a finite difference method with second-order accuracy in marching and fourth-order accuracy in the wall normal direction, hence, being free of any numerical viscosity, in contrast to the Navier–Stokes method.

3a) Conventionally the local, linear stability method[14] is applied, which solves the three-dimensional, compressible Orr–Sommerfeld stability equations using a finite difference scheme.

3b) Solely for one inifinite swept wing test case, the nonlocal, linear stability method (Schrauf, G., "A PSE Module—User's Guide and Tutorial," private communication, 2000) is applied, which solves the three-dimensional, compressible PSE using a finite difference scheme.

All Navier–Stokes computations are carried out using four mesh levels for the multigrid procedure, with 512×128 mesh volumes in the finest grid. The grid independence of the Navier–Stokes results for infinite swept wing configurations is presented in Ref. 8.

III. Description of Calculation Procedure

It is shown in Ref. 8 that the Navier–Stokes code for infinite, swept wing configurations delivers reliable laminar viscous layer results for stability computations on adapted meshes only. The quality of the viscous-layer prediction is documented by comparison with laminar results of a three-dimensional boundary-layer code, which uses the pressure distribution computed by the Navier–Stokes method as the boundary condition. The mesh adaption procedure represents such an untolerable engineering and computational demand that a different solution was found.[8] The stability analysis of the Navier–Stokes viscous layer was replaced without loss in accuracy by the stability analysis of three-dimensional boundary-layer results, evaluated from initial mesh Navier–Stokes wall pressure computations.

Wind-tunnel experiments on swept configurations are investigated, and the two N factor e^N method[8,9] is applied, where the limiting N factors for both the Tollmien–Schlichting and the stationary crossflow waves, representing the stability limit of the considered facility, are not known a priori. Actually, only crossflow-induced transition situations are considered, such that the limiting N factor for only stationary crossflow waves is of interest.

To begin, the limiting crossflow N factors of the different wind tunnels under consideration have to be determined. Navier–Stokes runs are executed imposing laminar flow on both upper and lower wing surfaces up to the location where the laminar boundary layer separates. (The possible existence of laminar separation bubbles is excluded from the present approach.) The three-dimensional laminar boundary-layer flow is evaluated[13] using the pressure distribution obtained from the Navier–Stokes solution. The viscous-layer data are analyzed by the local, linear stability method, applying the incompressible analysis.[14] Unstable stationary crossflow waves of constant spanwise wave number are computed as relevant disturbances. Their amplification rates are integrated, delivering the chordwise distribution of the crossflow N factor. The envelope N^*_{CF} factor curve is established, and the value of N_{CF} at the measured transition location X_{Tr}/C is determined. This process is repeated for all available experimental test conditions, that is, combinations of Reynolds number, angle of attack, and angle of sweep, yielding the limiting crossflow N factor N_{limit} as the mean of all N_{CF} values at measured transition.

Subsequently, the transition location is predicted, applying the earlier mentioned system of coupled codes, RANS, boundary layer, and stability, in an iterative manner. Conventionally, the transition location is determined, where the N^*_{CF} factors exceed the stability limit, that is, N_{limit}. Only in situations where the experimentally observed transition position is localized downstream of the computed laminar separation point, is the laminar separation point taken as transition location. The computed transition locations on upper and lower surfaces are transferred in a slightly underrelaxed manner to the subsequent Navier–Stokes run with transitional flow modeling[5,9] introduced to avoid strong viscous/inviscid interaction perturbations, which are present if point transition is applied.[5] The newly iterated transition location is then evaluated applying the earlier mentioned computational steps. Usually, the third iteration cycle delivers a converged solution.

IV. Results

Conventionally, it is assumed that the limiting N factors for both Tollmien–Schlichting and stationary crossflow waves are relatively constant for the specific, considered wind tunnel and for free-flight conditions. This general assumption implies the requirements that the limiting N factor is independent of wing cross-sectional shape, wing surface quality, sweep angle, Reynolds number, angle of attack, pressure distribution, and, up to transonic flow regimes, Mach number. It will be shown that, contrary to the general assumption, on one hand, unconventional wing section shapes and, on the other hand, different quality levels of the surface finish influence the crossflow N factor values, N_{CF}, at the measured transition location.

A. HQ26 Wing

The first investigated configuration is the infinite swept wing with the HQ26 profile (Fig. 1), designed for a tailless sailplane with low pitching moment values in the complete lift range of attached flow. The model was tested in the German Low Speed Wind Tunnel DLR, German Aerospace Research Center, Braunschweig.[15] The infinite swept wing flow was investigated for two different sweep angles $\lambda = 30$ and 45 deg, at different angles of attack $\alpha_s = -2.0$–8.6 deg and Reynolds numbers $Re = 1.8$–4.5×10^6. Figure 2 shows the measured pressure distribution compared to Navier–Stokes results for both sweep angles $\lambda = 30$ and 45 deg, angles of attack $\alpha_s = -2.0$ and 8.6 deg, and Reynolds numbers $Re \cong 3.0 \times 10^6$.

The N_{CF} factors for the different flow cases using the local, linear stability analysis are given in Fig. 3a. The values exhibit an unusual behavior because the N_{CF} factors for the lower and upper

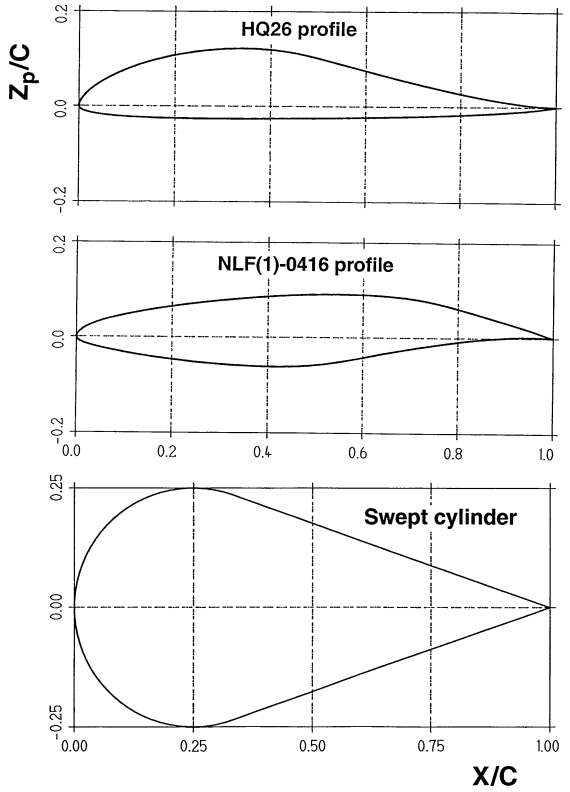

Fig. 1 Cross sections normal to the leading edge of the investigated configurations.

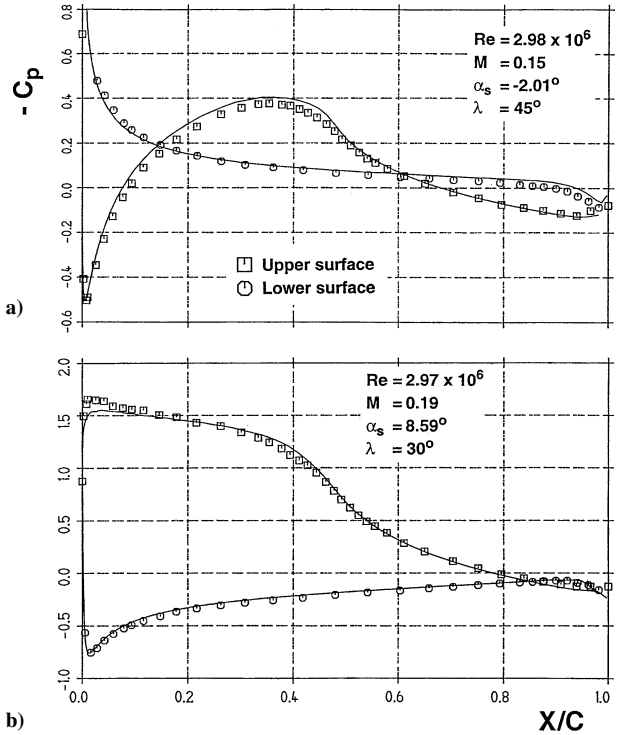

Fig. 2 Measured and computed pressure distribution for different angles of attack and sweep of the HQ26 infinite swept model.

wing surface differ nearly by a factor of two. This result was already obtained by Seitz.[15] Such a dramatic discrepancy of the N_{CF} factor values between lower and upper wing surfaces has never been observed in all related activities concerning the analysis of free-flight experiments.[16–22] (Other wind-tunnel campaigns, where upper and lower surface flows are investgated are not known.) The application of the nonlocal, linear PSE method (Schrauf, private communication) reduces the discrepancy slightly between lower and upper

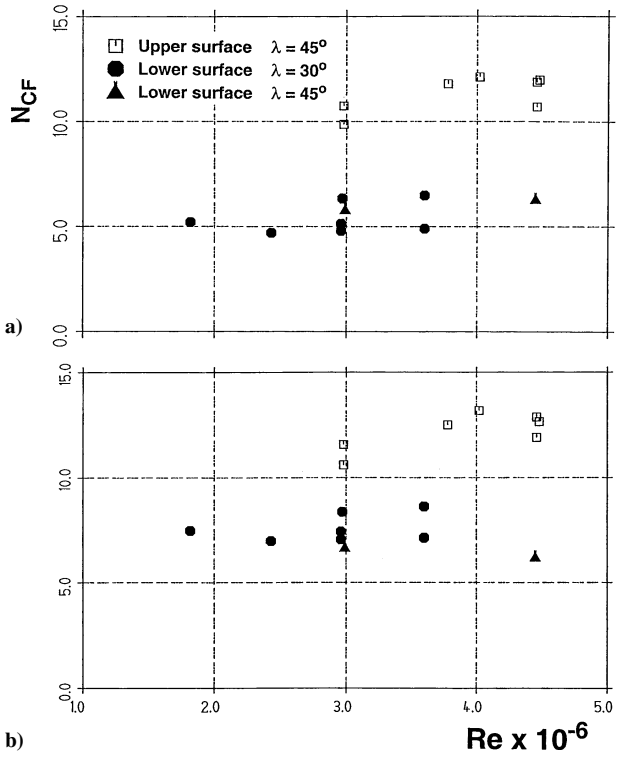

Fig. 3 N_{CF} factors on upper and lower surface of the HQ26 model using the linear stability method: a) local and b) nonlocal.

surface results, indeed, but does not resolve the problem (Fig. 3b). To investigate this phenomenon in further detail, two test cases on upper and lower wing surfaces were selected, which were tested at the same Reynolds number and exhibit comparable boundary-layer properties (Fig. 4). The pressure distribution is shown in Fig. 4a, the Reynolds number based on the incompressible value of the displacement thickness of the streamwise velocity profile in Fig. 4b, and the Reynolds number based on the incompressible value of the displacement thickness of the crossflow velocity profile in Fig. 4c. Although both displacement thickness Reynolds numbers are larger for the upper wing surface flow and, consequently, the N^*_{CF} factors are larger for the upper wing surface flow, calculated with the local, linear stability method,[14] transition is observed in the experiment farther downstream compared to the lower wing surface flow (Fig. 5). (Note that the streamwise velocity shape parameters are fairly comparable except close to separation on the upper wing surface.)

Because of the aerodynamic requirements mentioned earlier, the HQ26 wing has a fairly exceptional cross section (Fig. 1). The lower surface is almost flat, whereas the upper surface exhibits a large and nearly constant radius of curvature almost up to the midwing position. The curvature for the upper and lower wing surface is presented in Fig. 6. The extremely large difference in curvature appears to be the physical reason for the observed discrepancy. It is well known that stationary vortices are stabilized due to convexity of the surface and destabilized due to the concavity of the surface. Hence, the stability computations are now repeated using the local, linear and nonlocal, linear stability analysis with surface curvature effects included. The results are presented in Fig. 7. The N^*_{CF} factors are clearly reduced when including curvature effects for the upper wing surface flow (Fig. 7a), contrary to the almost negligible reduction of the N^*_{CF} factor on the wing lower surface (Fig. 7b). The results of Fig. 3 are repeated now in Fig. 8 with surface curvature effects included. Both results, local, linear and nonlocal, linear stability analysis, collapse for both wing surfaces in a fairly narrow band of N_{CF} factor values. When only the local, linear stability results are considered, the limiting N factor for stationary unstable waves is well represented by the mean value, $N_{limit} = 5$, indicated in Fig. 8a. When that value is applied for transition prediction, the transition locations compare fairly well with the experimental observations.

Figure 9 shows the results on the upper wing surface for a sweep angle $\lambda = 45$ deg, and Fig. 10 shows the results on the lower wing surface for sweep angles $\lambda = 45$ and 30 deg and different angles of attack. Obviously, the range of X/C values where transition is detected in the measurements is visibly larger on the lower wing surface, where the vortices are almost neutrally stable with respect to curvature effects.

It is important now to demonstrate the sensitivity of the results, such as drag coefficient, lift coefficient, and pressure distribution, on the values of the limiting N factor N_{limit}. The flow cases given in Fig. 2 are recomputed for two values of N_{limit}: $N_{\text{limit}} = 5$ and $N_{\text{limit}} = 10$. The correspondent transition locations on upper and lower surfaces are given in Table 1. The flow case with the negative angle of attack $\alpha = -2.01$ deg exhibits the same transition location on the lower surface for both values of N_{limit} because transition is fixed immediately downstream of the suction peak, where the laminar boundary layer separates. Similarly, the transition location on the upper surface for the second flow case is identical, $X_{\text{Tr}}/C = 0.3644$, for both values of N_{limit}. There is no crossflow exitation present so that transition is also fixed here at the laminar flow separation location.

As can be seen from Table 1, the wing section lift coefficient C_L and the wing section pressure drag coefficient C_{Dp} are both mildly influenced by the N_{limit} variation, contrary to the wing section friction drag coefficients C_{Df}. As expected, the wing section friction drag coefficient and, consequently, also the wing section total drag

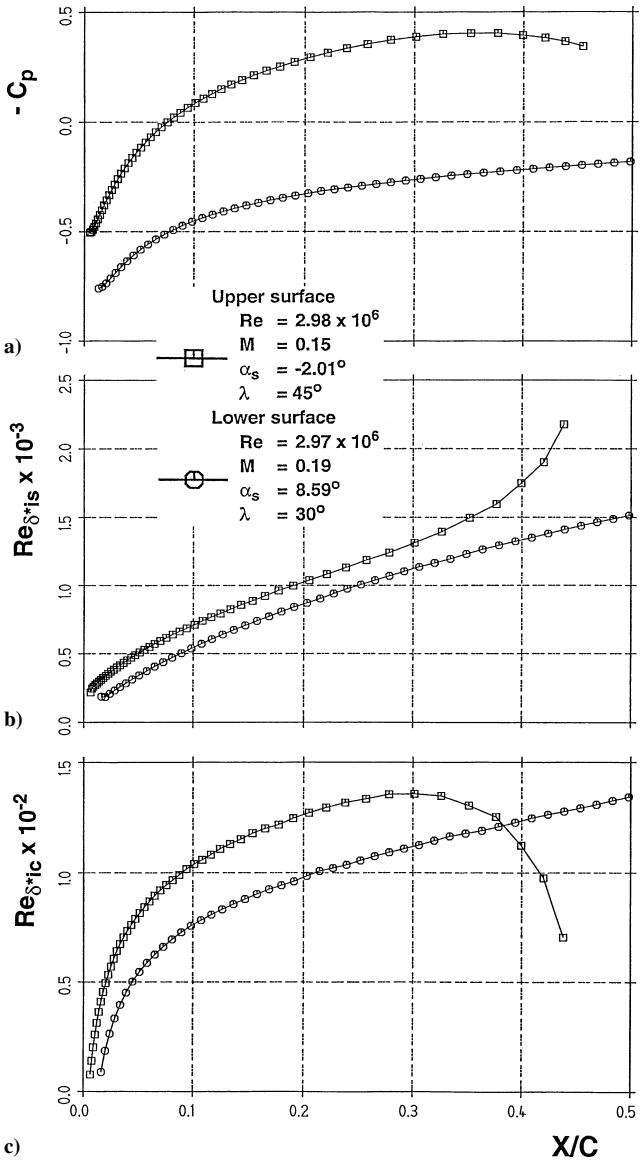

Fig. 4 Computed flow values on upper and lower surface of the HQ26 model for comparable Reynolds numbers: a) pressure distribution, b) Reynolds number based on displacement thickness of the streamwise velocity profile, and c) Reynolds number based on displacement thickness of the cross-flow velocity profile.

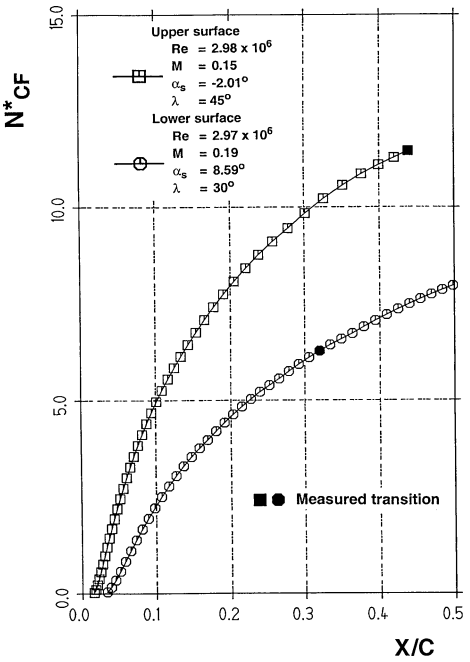

Fig. 5 N^*_{CF} factor distribution on upper and lower surface of HQ26 model.

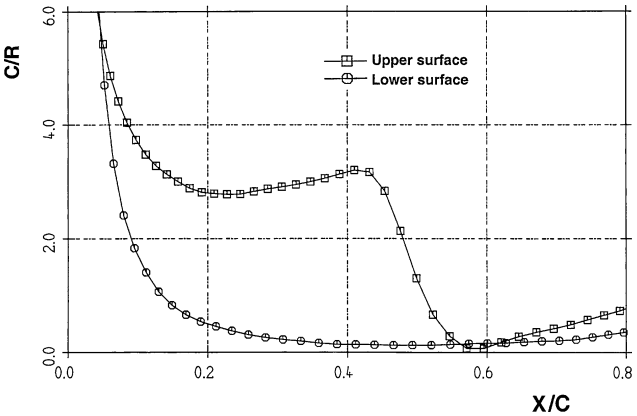

Fig. 6 Curvature on upper and lower surface of HQ26 model.

Table 1 Dependence of transition location and aerodynamic coefficients on the value of N_{limit}

α	λ	X_{Tr}/C upper surface	X_{Tr}/C lower surface	$C_{D\text{tot}}$	C_{Df}	C_{Dp}	C_L	N_{limit}
−2.01	45.0	0.309	0.006	0.00567	0.00440	0.00127	−0.0109	10.0
−2.01	45.0	0.100	0.006	0.00641	0.00506	0.00135	−0.0115	5.0
8.59	30.0	0.3644	0.779	0.00632	0.00337	0.00295	0.95134	10.0
8.59	30.0	0.3644	0.230	0.00716	0.00436	0.00280	0.95535	5.0

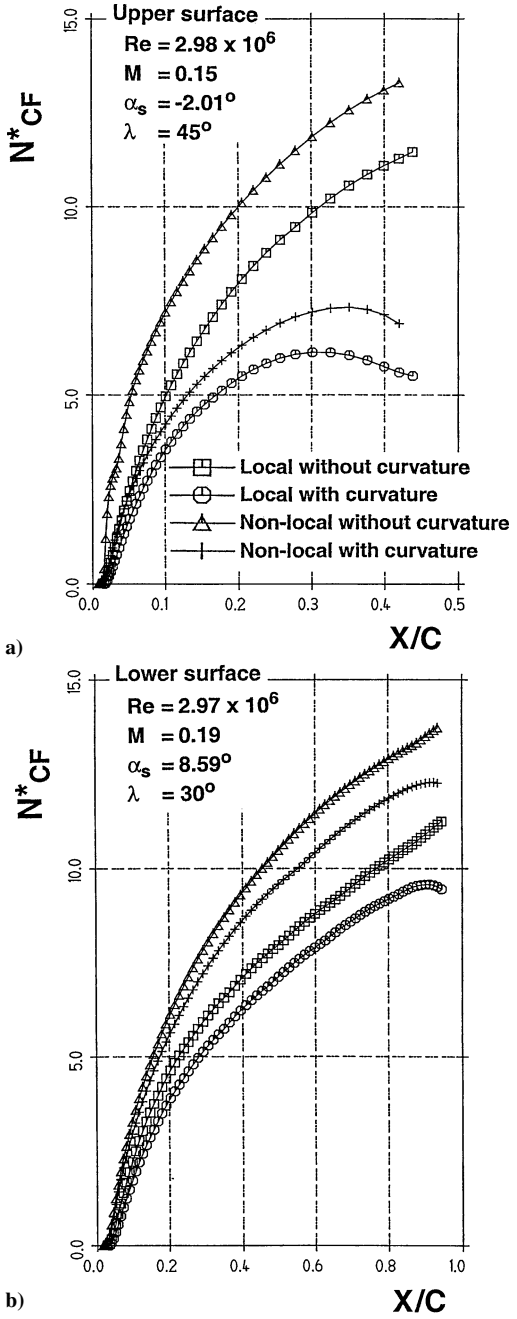

Fig. 7 N^*_{CF} factor distribution of HQ26 model with and without surface curvature on a) upper surface and b) lower surface.

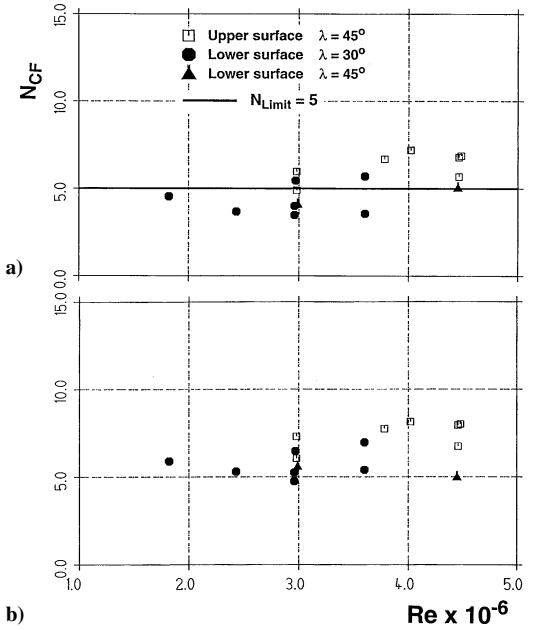

Fig. 8 N_{CF} factors on upper and lower surface of the HQ26 model using linear stability method with curvature effects: a) local and b) nonlocal.

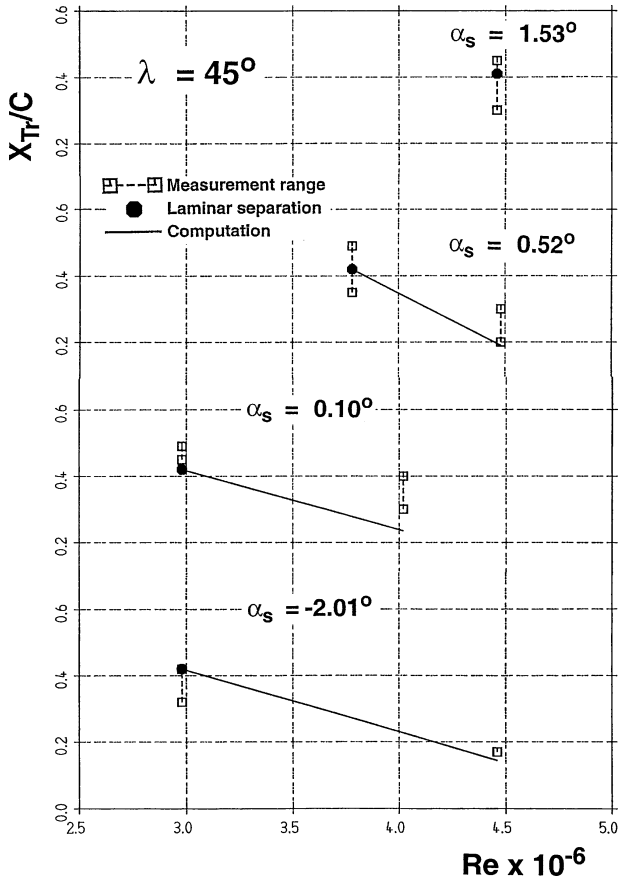

Fig. 9 Measured and computed transition locations on the upper surface on HQ26 model.

coefficient $C_{D\text{tot}}$ are larger for the lower value of N_{limit}. Correspondingly, the difference in the pressure distribution (Fig. 11) due to the N_{limit} variation is only marginal for both flow cases.

Concluding, the conventional e^N method for crossflow-induced transition, that is, the application of the local, linear stability analysis and one constant value, N_{limit}, for the considered wind tunnel, is applicable only for conventional wings with comparable surface curvature on both upper and lower wing surfaces, such as all commercial aircraft wings. However for unconventional sailplane wings, such as the HQ26 wing, the value of N_{limit} is also geometry dependent. This dependence, however, can be circumvented if the local, linear stability analysis with surface curvature effects included is used for the evaluation of the limiting N factor N_{limit}.

B. NLF(1)-0416 Wing

The infinite swept wing model equipped with the NLF(1)-0416 airfoil[23] (Fig. 1) was tested in the Arizona State University Unsteady Low Speed Wind Tunnel (UWT)[24] at a sweep angle $\lambda = 45$ deg and an angle of attack $\alpha_n = -4$ deg, in the Reynolds number range $Re = 1.9$–3.7×10^6. Radeztsky et al.[24] measured the transition location on the upper wing surface dependent on the quality of the surface finish. Figure 12 shows the measured pressure distribution compared to the Navier–Stokes result on the upper wing surface. The pressure was measured at the lower and upper end of the wing model, which produces continously accelerated flow up to the chordwise station $X/C = 0.7$. As can be seen, small spanwise

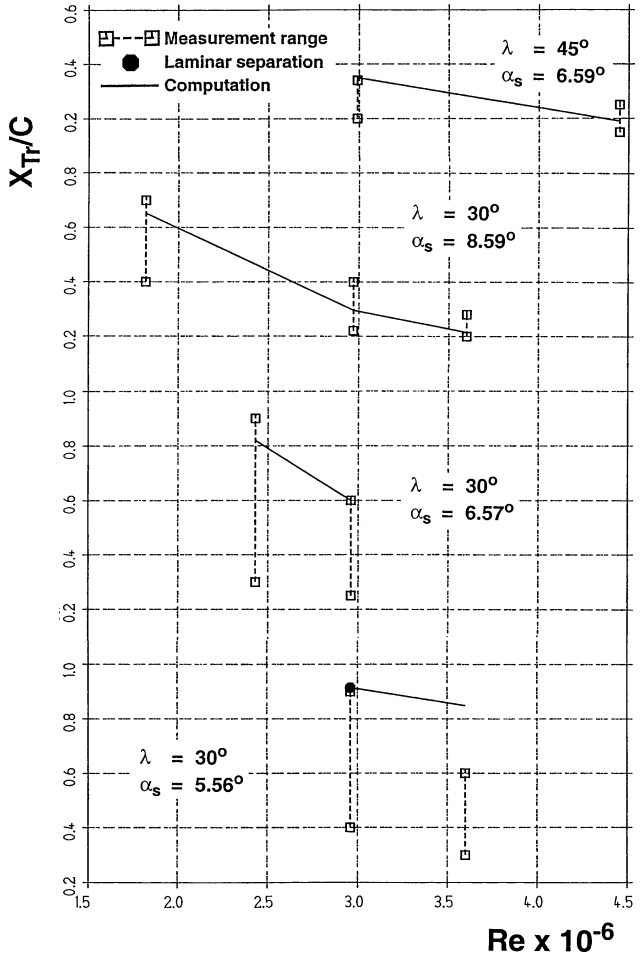

Fig. 10 Measured and computed transition locations on the lower surface of HQ26 model.

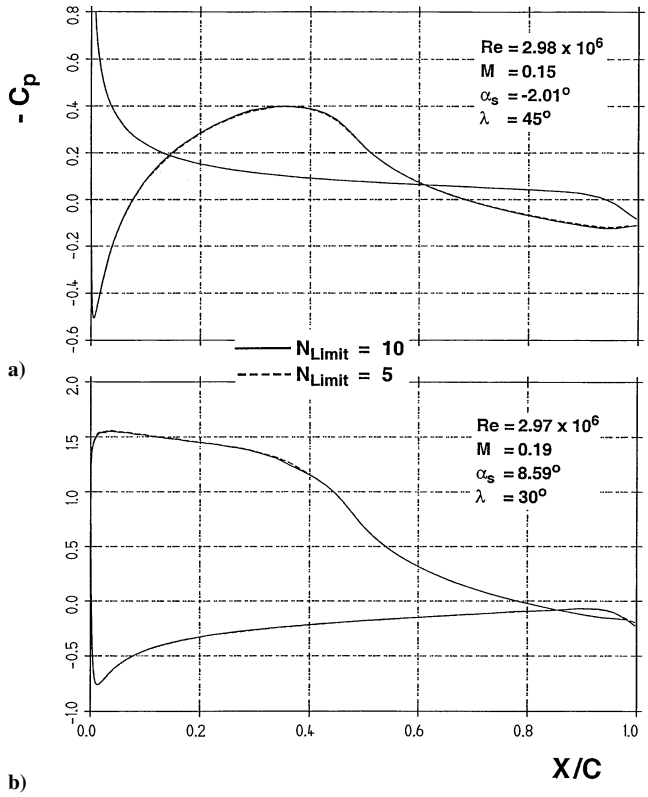

Fig. 11 Influence of the value of N_{limit} on the pressure distribution.

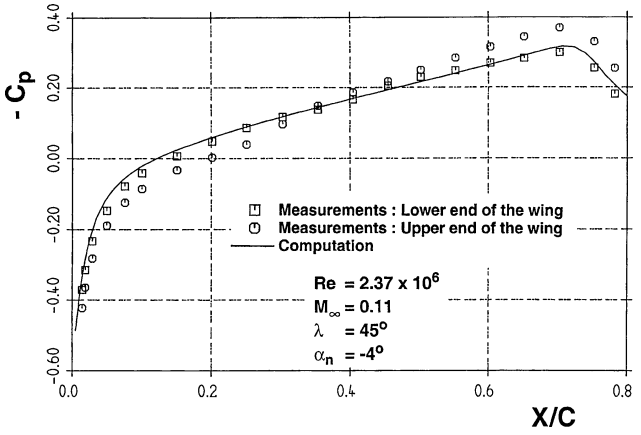

Fig. 12 Measured and computed pressure distribution on upper surface of NLF(1)-0416 infinite swept model.

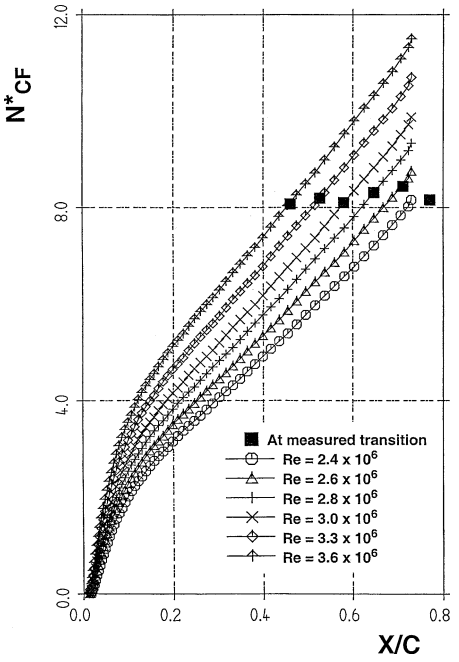

Fig. 13 N^*_{CF} factor distribution for different Reynolds numbers on the upper surface of the NLF(1)-0416 model including data at the measured transition locations for final surface finish.

pressure gradients are present. The Navier–Stokes results reproduce almost identically the measurements at the lower end of the wing. In Fig. 13, the N^*_{CF} factor curves for the different Reynolds numbers are presented. Furthermore, the measured transition locations are indicated, which were measured for the final surface polish with roughness heights of at most 0.25 μm. The N_{CF} factor values obtained for the different surface qualities, that is, final polish 0.25 μm, first polish 0.5 μm, and the paint 9 μm, are shown in Fig. 14. Crossflow instabilities are known to be extremely sensitive to roughnesses in the leading-edge region. As expected, the values of the limiting N factor N_{limit} increase with reduced roughness height. The values of the limiting crossflow N factor $N_{\text{limit}} = 8.3$, $N_{\text{limit}} = 7.6$, and $N_{\text{limit}} = 6.0$, respectively, are also indicated in Fig. 14. Applying these limiting N factors produces computational results for the transition prediction in close agreement with the experimental findings (Fig. 15).

Concluding, the conventional e^N method, that is, one constant value of N_{limit} for the considered wind tunnel, is only applicable if the surfaces of the investigated wings have a comparable quality of the surface finish.

C. Cylinder Model

Finally, it will be demonstrated for flows in the vicinity of the leading edge of a swept wing that the e^N method is capable of

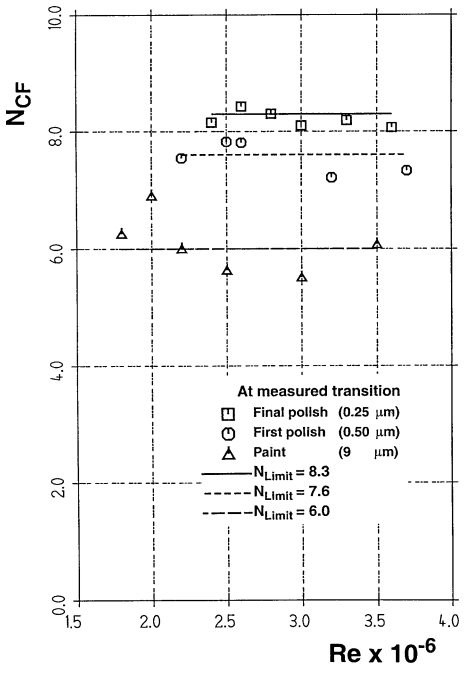

Fig. 14 N_{CF} factors on upper surface of NLF(1)-0416 model for different surface qualities.

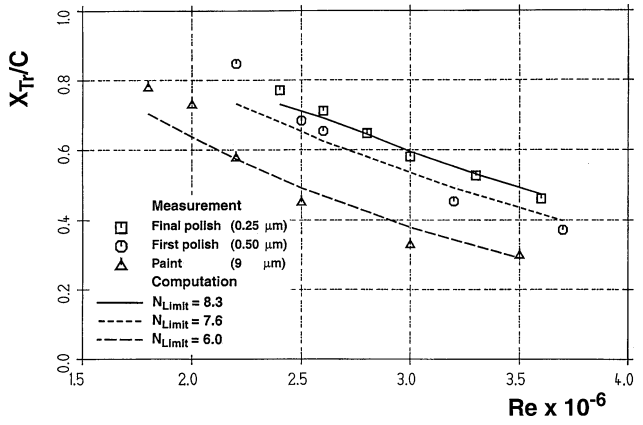

Fig. 15 Measured and computed transition locations on upper surface of NLF(1)-0416 model for different surface qualities.

reproducing the well-known boundaries between noncontaminated, that is, fully laminar attachment line flows, and fully contaminated turbulent attachment line flows.

The investigated configuration is the cylinder model of Poll[25] (Fig. 1), tested for sweep angles $\lambda = 53$–71 deg and Reynolds numbers $Re = 0.9$–1.7×10^6. Figure 16 gives the measured pressure distribution for sweep angles $\lambda = 55$, 63, and 71 deg compared to the potential theory and Navier–Stokes results. As can be seen, the Navier–Stokes method only produces results in basic agreement. Figure 17 is reproduced from Ref. 25 and shows the measured transition locations as a function of Reynolds number and sweep angle. The N_{CF} factors are presented in Fig. 18 for the different sweep angles as a function of the Reynolds number. In Fig. 18a, the N_{CF} factors are relatively constant for sweep angles $\lambda = 53$, 55, and 57.9 deg, which allow the estimate of $N_{\text{limit}} = 6.8$. However, for larger sweep angles, the N_{CF} factors decay gradually with increasing sweep and nearly vanish for the largest sweep angles (Fig. 18b). The cause for the decay of the N_{CF} factors is the progressive increase of contamination in the laminar cylinder attachment line flow, which starts in the actual test cases for sweep angles $\lambda > 58$ deg. Pfenninger[26] proposed a criterion for the onset of laminar boundary-layer contamination on swept wings, which depends on the balance of the pressure and inertia forces against the viscous forces. The

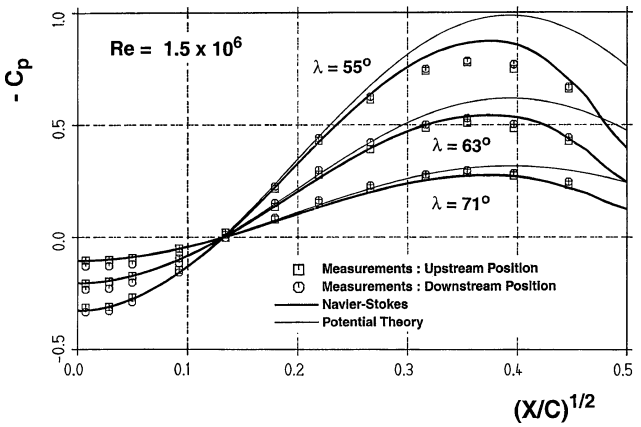

Fig. 16 Measured and computed pressure distribution for different sweep angles of cylinder model.

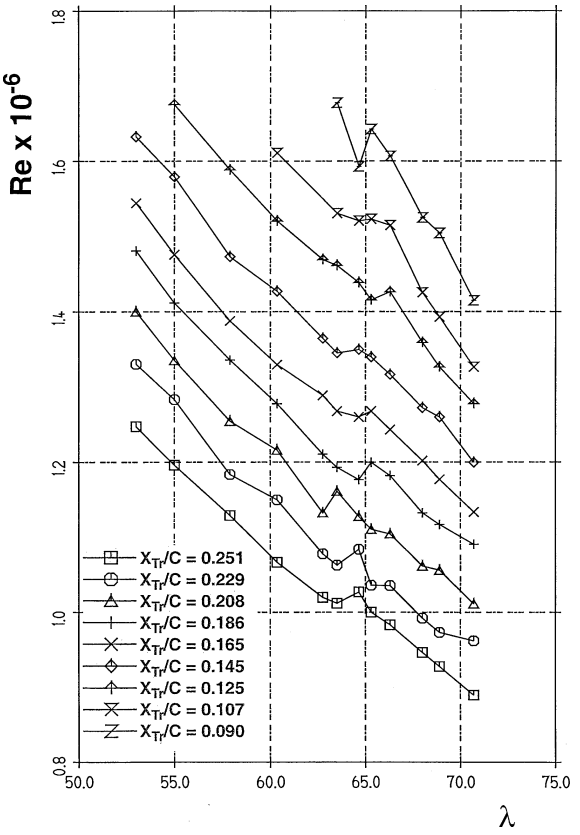

Fig. 17 Reynolds number as a function of sweep angle for different measured transition locations on cylinder model.

Reynolds number $\bar{R}e$ appears as a meaningful parameter in defining the conditions necessary for contamination, when triggered by leading-edge perturbations.[26] The definition of Reynolds number $\bar{R}e$ is given by

$$\bar{R}e = W_\infty \Big/ \left[\left(\frac{\mu}{\rho} \frac{\mathrm{d}u_e}{\mathrm{d}s} \right)_{\text{al}} \right]^{\frac{1}{2}} \tag{1}$$

It is shown in Ref. 26 that $\bar{R}e$ can be expressed by Re_θ:

$$Re_\theta = 0.405 \bar{R}e \tag{2}$$

In Fig. 19, the values of Reynolds number Re_θ are plotted for all test cases vs the Reynolds number Re with the sweep angle λ as parameter. Furthermore, two limits are indicated in Fig. 19, which mark the onset of contamination (continous line) and the start of fully contaminated turbulent attachment line flow (dashed line). The limits are based on experimental observations and are given by[27]

$$Re_\theta = 100 \pm 4 \tag{3}$$

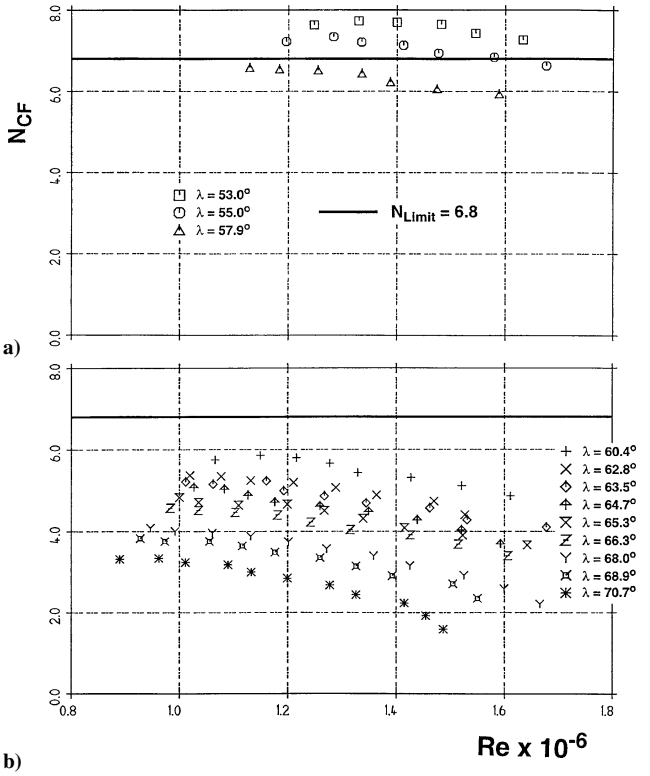

Fig. 18 N_{CF} factors on the cylinder model as a function of the Reynolds number: a) laminar leading-edge flow and b) contaminated leading-edge flow.

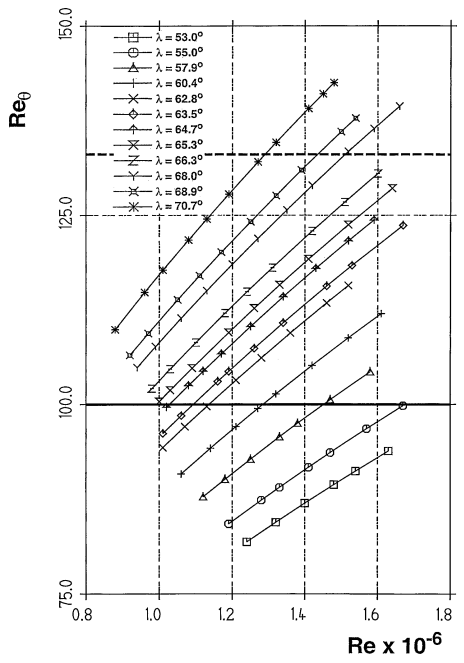

Fig. 19 Reynolds number based on the momemtum loss thickness of the attachment line flow as a function of Reynolds number with sweep angle as a parameter.

for the lower limit and

$$Re_\theta = 133 \pm 9 \tag{4}$$

for the upper limit.

As can be seen, these limits fit fairly well with the results of Fig. 18. The Reynolds number Re_θ values for sweep angles $\lambda = 53$, 55, and 57.9 deg are smaller than the lower limit [Eq. (3)] and can be considered as noncontaminated laminar attachment line flows (Fig. 18a). All Reynolds number Re_θ values for sweep angles $\lambda \geq 60$ deg are larger than the lower limit, and increasing

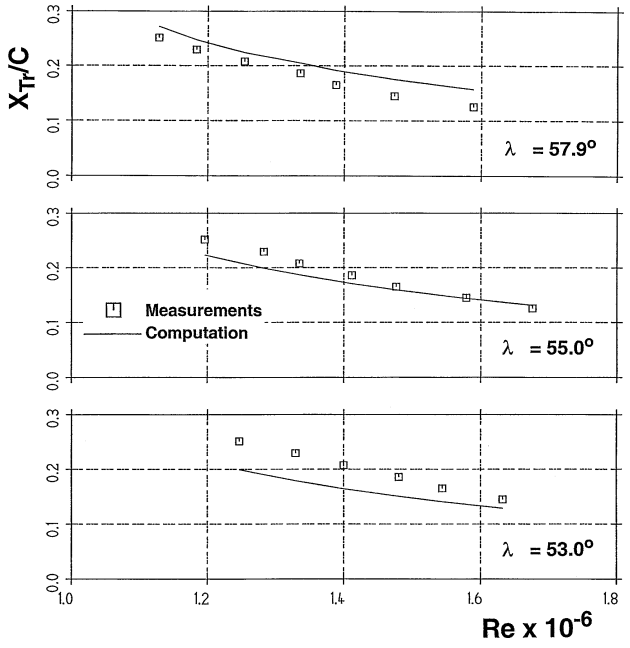

Fig. 20 Measured and computed transition locations on the cylinder model for different angles of sweep.

contamination takes place (Fig. 18b). For the largest sweep angles $\lambda \geq 68$ deg, the Reynolds number Re_θ values exceed the upper limit [Eq. (4)] fully turbulent attachment line flow can be expected, or in terms of the crossflow stability analysis, vanishing N_{CF} factors. Indeed, the actual approach shows fairly small N_{CF} factors in this range of sweep angles (Fig. 18b). Finally, the transition location prediction (Fig. 20) compares fairly well for noncontaminated laminar flow with experimental findings on the swept cylinder model for sweep angles $\lambda = 53$, 55, and 57.9 deg.

V. Conclusions

The results of a RANS method for two infinite swept wings and a cylinder model coupled to a boundary-layer and transition prediction method based on the e^N approach are presented. Conventionally, the limiting N factors for both Tollmien–Schlichting and crossflow instabilities are assumed to be relatively constant for a specific windtunnel or for free-flight conditions. This general assumption implies the requirements that the values of the limiting N factors are independent of wing cross-sectional shape, wing surface quality, sweep angle, Reynolds number, angle of attack, pressure distribution, and, up to transonic flow regimes, Mach number. The comparison with experiments of the two infinite swept wing configurations shows, first, that extremely different curvatures on upper and lower wing surface and, second, that different qualities of the wing surface finish, that is, different surface roughness levels, influence the value of the limiting crossflow N factor. Only the actually investigated, unconventional sailplane wing exhibits extremely different curvatures on upper and lower wing surfaces, contrary to all commercial aircraft wings. Hence, the conventional e^N method remains applicable, if supplementary requirements are introduced, namely, first, that the investigated wings show comparable curvatures on both upper and lower wing surface and, second, that the wings exhibit a comparable surface finish.

Last, the computations of flows around the cylinder model compared to experimental results document that the e^N method is capable to deal with the leading-edge contamination problem. Both flow condition boundaries, where contamination starts to influence the laminar leading-edge flow and where fully contaminated turbulent flow is to be expected, are well predicted by the e^N method.

Acknowledgment

This research has been supported in part by the European Union in the Application of Hybrid Laminar Flow Technology on Transport

Aircraft program in Basic Research for Industrial Technologies/ European Research in Advanced Materials.

References

[1]Smith, A. M. O., and Gamberoni, N., "Transition, Pressure Gradient and Stability Theory," Douglas Aircraft Co., Rept. ES 26388, Long Beach, CA, April 1956.

[2]van Ingen, J. L., "A suggested Semi-Empirical Method for the Calculation of the Boundary Layer Transition Region," Dept. of Aerospace Engineering, Rept. VTH-74, Univ. of Delft, Delft, The Netherlands, Oct. 1956.

[3]Arnal, D., and Casalis, G., "Laminar–Turbulent Transition Prediction in Three-Dimensional Flows," *Progress in Aerospace Sciences*, Vol. 36, 2000, pp. 173–191.

[4]Stock, H. W., and Haase, W., "A Feasibilty Study of e^N Transition Prediction in Navier–Stokes Methods for Two Dimensinal Airfoil Computations," *AIAA Journal*, Vol. 37, No. 10, 1999, pp. 1187–1196.

[5]Stock, H. W., and Haase, W., "Navier–Stokes Airfoil Computations with e^N Transition Prediction Including Transitional Flow Regions," *AIAA Journal*, Vol. 38, No. 11, 2000, pp. 2059–2066.

[6]Stock, H. W., "Airfoil Validation Using Coupled Navier–Stokes and e^N Transition Prediction Methods," *Journal of Aircraft*, Vol. 39, No. 1, 2002, pp. 51–58.

[7]Stock, H. W., "Wind-Tunnel-Flight Correlation for Laminar Wings in Adiabatic and Heating Flow Conditions," *Aerospace Science and Technology* Vol. 6, 2002, pp. 245–257.

[8]Stock, H. W., "Infinite Swept Wing RANS Computations with e^N Transition Prediction—Feasibility Study," DLR, German Aerospace Research Center, DLR-IB 124-2003/12, Braunschweig, Germany, Feb. 2003.

[9]Stock, H. W., "Infinite Swept Wing RANS Computations with e^N Transition Prediction—Validation Study," DLR, German Aerospace Research Center, DLR-IB 124-2003/13, Braunschweig, Germany, Feb. 2003.

[10]Haase, W., "EUROVAL—A European Initiative on Validation of CFD Codes," *Notes on Numerical Fluid Mechanics*, Vol. 42, Vieweg Verlag, Braunschweig, Germany, 1992, pp. 82–87.

[11]Leicher, S., Höld, R., and Grashof, J., "MEGAFLOW Final Report," DaimlerChrysler, Rept. DASA-S-R-1794, Munich, March 1999.

[12]Baldwin, B. S., and Lomax, H., "Thin Layer Approximation and Algebraic Model for Separated Turbulent Flows," AIAA Paper 78-257, 1978.

[13]Horton, H. P., and Stock, H. W., "Computation of Compressible, Laminar Boundary Layers on Swept, Tapered Wings," *Journal of Aircraft*, Vol. 32, No. 6, 1995, pp. 1402–1405.

[14]Schrauf, G., "An Efficient Solver of the Eigenvalue Problem of the Linear Stability Equations for Three-Dimensional, Compressible Boundary Layer Flows," *6th DGLR-Fach-Symposium (Strömungen mit Ablösung)*, Deutsche Gesellschaft für Luft- und Raumfahrt e.V., Rept. DGLR-REP. 88-05, Bonn, 1988, pp. 18–27.

[15]Seitz, A., "Ermittlung des Querströmungs *N* Faktors zur Umschlagvorhersage im Niedergeschwindigkeitswindkanal Braunschweig (NWB)," DFVLR, Rept. DFVLR-IB/129-89/26, Braunschweig, Germany, Aug. 1989.

[16]Schrauf, G., "Transition Prediction Using Different Linear Stability Analysis Strategies," AIAA Paper 94-1848, June 1994.

[17]Henke, R., Münch, F. X., and Quast, A.,"Natural Laminar Flow: A Wind Tunnel Test Campaign and Comparison with Free Flight Test Data," AIAA Paper 90-3045, Aug. 1990.

[18]Horstmann, K. H., Redeker, G., Quast, A., Dressler, U., and Bieler, H., "Flight Tests with a Natural Laminar Flow Glove on a Transport Aircraft," AIAA Paper 90-3044, Aug. 1990.

[19]Schrauf, G., Perraud, J., and Lam, F., "Comparison of Boundary-Layer Transition Predictions Using Free-Flight Test Data," *Journal of Aircraft*, Vol. 35, No. 6, 1998, pp. 891–897.

[20]Schrauf, G., "Linear Stability Theory Applied to Wind Tunnel and Flight Experiments," *Proceedings of the 4th European Computational Conference, ECCOMAS 98*, Vol. 2, Wiley, Chichester, England, U.K., 1998, pp. 126–131.

[21]Schrauf, G., Perraud, J., Lam, F., Stock, H. W., Vitiello D., and Abbas, A., "Transition Prediction with Linear Stability Theory—Lessons Learned from the ELFIN F100 Flight Demonstrator," 2nd European Forum on Laminar Flow Technology, Association Aeronautique et Astronautique de France, Paris, Paper 8.5, June 1996.

[22]Arnal, D., and Bulgubure, C., "Drag Reduction by Boundary-Layer Laminarisation," *La Recherche Aerospatiale*, Vol. 3, 1996, pp. 157–165.

[23]Somers, D. M., and Horstmann, K. H., "Design of a Medium-Speed Natural-Laminar-Flow Airfoil for Commuter Aircraft Applications," DFVLR, Rept. DFVLR-IB/29-85/26, Braunschweig, Germany, July 1985.

[24]Radeztsky, R. H., Reibert, M. S., Saric, W. S., and Takagi, S., "Effect of Micron-Sized Roughness on Transition in Swept-Wing Flows," AIAA Paper 93-0076, Jan. 1993.

[25]Poll, D.I.A., "Some Observations of the Transition Process on the Windward Face of a Long Yawed Cylinder," *Journal of Fluid Mechanics,* Vol. 150, 1985, pp. 329–356.

[26]Pfenninger, W., "Flow Phenomena at the Leading Edge of Swept Wings," *Recent Developments in Boundary-Layer Research*, AGARDograph 97, Pt. 4, 1965, pp. 1–41.

[27]Arnal, D., and Juillen, J. C., "Leading Edge Contamination and Relaminarization on a Swept Wing at Incidence," 4th Symposium on Numerical and Physical Aspects of Aerodynamic Flows, California State Univ., Long Beach, CA, 1989.

R. So
Associate Editor